

Computational Optical Coherence and Statistical Optics

Computational Optical Coherence and Statistical Optics

Milo W. Hyde IV

SPIE PRESS
Bellingham, Washington USA

Library of Congress Cataloging-in-Publication Data

Names: Hyde, Milo W., author.

Title: Computational optical coherence and statistical optics / Milo W. Hyde, IV,
Air Force Institute of Technology.

Description: Bellingham, Washington : SPIE—The International Society for
Optical Engineering, 2023. | Includes bibliographical references and index.

Identifiers: LCCN 2022037732 | ISBN 9781510657175 (paperback) |
ISBN 9781510657168 (pdf)

Subjects: LCSH: Coherence (Optics)—Computer simulations. | Coherence (Optics)—
Statistical methods.

Classification: LCC QC476.C6 H93 2023 | DDC 535/.2—dc23/eng20221209

LC record available at <https://lccn.loc.gov/2022037732>

Published by

SPIE

P.O. Box 10

Bellingham, Washington 98227-0010 USA

Phone: +1 360.676.3290

Fax: +1 360.647.1445

Email: books@spie.org

Web: www.spie.org

This book is declared a work of the United States government and is not subject to
copyright. Publication year: 2023.

All rights reserved. No part of this publication may be reproduced or distributed in
any form or by any means without written permission of the publisher.

The content of this book reflects the work and thought of the author. Every effort has
been made to publish reliable and accurate information herein, but the publisher is
not responsible for the validity of the information or for any outcomes resulting from
reliance thereon.

Printed in the United States of America.

First printing 2023.

For updates to this book, visit <http://spie.org> and type “PM356” in the search field.

SPIE.

Contents

<i>Preface</i>	<i>xiii</i>
<i>Acronyms</i>	<i>xix</i>
1 Scalar Partially Coherent Sources: Theoretical Foundations	1
1.1 Review of Scalar Diffraction Theory	1
1.1.1 Maxwell's Equations and the Scalar Wave Equation	1
1.1.2 Solution of the Scalar Wave Equation and the Plane Wave Spectrum	3
1.1.3 Fresnel and Fraunhofer Diffraction	7
1.2 First-Order Field and Irradiance Statistics	8
1.2.1 Thermal and Pseudo-Thermal Light	8
1.2.2 Probability Density Function of the Irradiance	12
1.3 Second-Order Field Statistics	14
1.3.1 Mutual Coherence Function	14
1.3.2 Cross-Spectral Density Function	19
1.3.3 Propagation of the Cross-Spectral Density Function	21
1.3.4 Coherent-Modes Representation	22
1.3.5 Superposition Rule	24
1.3.6 Models of the Cross-Spectral Density Function	26
1.3.7 The van Cittert–Zernike Theorem	34
1.4 Second-Order Irradiance Statistics	36
1.4.1 Covariance of Irradiance	37
1.4.2 Statistics of Integrated Irradiance	39
1.4.3 Intensity Interferometry	44
References	46
2 Simulating Random Scalar Fields	55
2.1 Coherent-Modes Representation	57
2.1.1 Simulation Methods	58
2.1.2 Gaussian Schell-Model Source	64
2.1.3 I_m -Bessel Correlated Source	71
2.2 Superposition Rule: Pseudo-Modes	82
2.2.1 Simulation Methods	83
2.2.2 Schell-Model Sources	86

2.2.3	Self-Focusing Non-uniformly Correlated Sources	91
2.3	Superposition Rule: Thermal and Pseudo-Thermal Light	95
2.3.1	Simulation Method	97
2.3.2	Schell-Model Sources	101
2.3.3	Self-Focusing Non-uniformly Correlated Sources	105
	References	115
3	Electromagnetic Partially Coherent Sources: Theoretical Foundations	123
3.1	Review of Electromagnetic Theory	123
3.1.1	Electromagnetic Plane Wave Spectrum	123
3.1.2	Polarization Ellipse	130
3.1.3	Jones Vectors, Stokes Parameters, and the Poincaré Sphere	133
3.2	First-Order Field and Irradiance Statistics	138
3.2.1	Partially Polarized Thermal and Pseudo-Thermal Light	138
3.2.2	Probability Density Functions of Stokes Parameters	143
3.3	Second-Order Field Statistics	147
3.3.1	Beam Coherence-Polarization Matrix	147
3.3.2	Cross-Spectral Density Matrix	149
3.3.3	Propagation of the Cross-Spectral Density Matrix	150
3.3.4	Coherent-Modes Representation	152
3.3.5	Superposition Rule	154
3.3.6	Models of the Cross-Spectral Density Matrix	155
3.4	Second-Order Irradiance Statistics	160
3.4.1	Covariance of Irradiance	161
	References	164
4	Simulating Random Electromagnetic Fields	175
4.1	Coherent-Modes Representation: Bimodal Expansions	176
4.1.1	Simulation Method	177
4.1.2	Electromagnetic Gaussian Schell-Model Source	182
4.2	Superposition Rule: Pseudo-Modes	190
4.2.1	Simulation Method	191
4.2.2	Electromagnetic Schell-Model Sources	203
4.2.3	Electromagnetic Self-Focusing Non-uniformly Correlated Sources	209
4.3	Superposition Rule: Thermal and Pseudo-thermal Light	220
4.3.1	Simulation Method	221
4.3.2	Electromagnetic Schell-Model Sources	231
4.3.3	Electromagnetic Self-Focusing Non-uniformly Correlated Sources	237
	References	260

5	Application Examples	265
5.1	Young's Experiment	265
5.1.1	Theory	265
5.1.2	Simulation	272
5.2	Michelson Interferometer	279
5.2.1	Theory	281
5.2.2	Simulation	287
5.3	The van Cittert–Zernike Theorem	294
5.3.1	Beam Shaping with Random Scalar Fields	295
5.3.2	Polarization Control with Random Electromagnetic Fields	301
5.4	The Hanbury Brown and Twiss Effect	307
5.4.1	Theory	309
5.4.2	Simulation	314
5.5	Imaging with Partially Coherent Light	318
5.5.1	Theory	318
5.5.2	Simulation	321
	References	330
6	Pulsed Partially Coherent Fields	337
6.1	Review of Basic Theory	338
6.1.1	Coherent-Modes Representation	339
6.1.2	Superposition Rule	340
6.1.2.1	Pseudo-modal expansions	340
6.1.2.2	Superposition-rule method	342
6.2	Superposition Rule: Thermal and Pseudo-Thermal Light	344
6.2.1	Schell-Model Pulsed Beams	347
6.2.2	Non-uniformly Correlated Pulsed Beams	357
6.2.3	Spatiotemporal Coupling: Twisted Space-Time Beams	375
	References	394
Appendix A	Numerical Diffraction Using the Collins Formula	399
A.1	The Collins Formula	400
A.2	Sampling Analysis	402
A.3	Example	406
	References	410
Appendix B	Simulating Spatially Incoherent Sources	411
B.1	Theory	412
B.2	Example	415
	References	422
Appendix C	MATLAB[®] Code	425
C.1	Chapter II	426
C.2	Chapter IV	443
C.3	Chapter V	454

C.4 Chapter VI	468
C.5 Appendix A	485
C.6 Appendix B	488
Reference	490
<i>Index</i>	491

☞ The supplemental material for this book is available in Appendix C and for download here: https://spie.org/Samples/Pressbook_Supplemental/PM356_sup.zip

Preface

The field of optics can generally be divided into four subfields or disciplines, namely, geometrical, wave, statistical, and quantum optics. Geometrical or ray optics is by far the oldest and most mature subfield, having been studied since the time of Fermat and Newton. Geometrical optics models light as a ray and is accurate in the asymptotic limit as the wavelength goes to zero. As a result, geometrical optics does not accurately predict phenomena such as diffraction (although it can be extended to include such phenomena via the geometrical theory of diffraction and the uniform theory of diffraction). Wave optics—developed by giants like Fresnel, Young, Maxwell, Rayleigh, and Sommerfeld—includes diffraction, interference, and all other wave phenomena and is the second most mature discipline. The most popular application of wave optics theory is Fourier optics, so much so that the two are now synonymous. Both geometrical and wave optics are extensively used in optical design and have been the subject of numerous theoretical and computational textbooks.

Statistical optics, as it is commonly defined, extends both geometrical and wave optics to include random optical sources, propagation through or scattering from random media, and detector noise. Major contributors to the discipline include Wolf, Goodman, Tatarskii, and Ishimaru. Indeed, Wolf (co-authored with Mandel) and Goodman, respectively, are the authors of what are universally considered the definitive texts on the subject: *Optical Coherence and Quantum Optics* and *Statistical Optics*, now in its second edition. These books present the theoretical foundations of statistical optics and classical optical coherence in excellent physical detail.

Quantum optics arose as a discipline around the time of the first lasers in the 1960s. It includes all aspects of geometrical, wave, and statistical optics and accurately predicts the interaction of individual photons with atoms, the inner workings of lasers, squeezed light states, photoelectric detection, etc. Significant contributors to quantum optics include some of the most brilliant minds in physics—Einstein, Schrödinger, Bohr, Heisenberg, Born, and Mandel. Applications that employ statistical and quantum optics theory are legion: in the case of the former, adaptive optics, optical communications, optical tweezing, directed energy, and remote sensing, and in the latter, lasers,

quantum communications, and quantum computing. This list is by no means all-inclusive.


While some of the technologies and applications listed above are well established, many are still in development, and consequently, active areas of research. Statistical optics is a little more mature in this regard. In recent years, statistical optics and classical optical coherence theory have been applied to engineer and synthesize random fields for use in specific applications, many of which are mentioned above. Indeed, techniques to physically generate optical fields with prescribed correlation or coherence properties can be found throughout the published literature. Two recent papers in *Progress in Optics* entitled “Generation of partially coherent beams” (*Prog. Opt.* 2017, **62**, 157–223) and “Applications of optical coherence theory” (*Prog. Opt.* 2020, **65**, 43–104) provide excellent summaries of these topics. As novel technologies and applications increasingly exploit optical coherence, accurate simulation of stochastic optical fields becomes critically important. Recent books on statistical optics have started to include sections on simulating random optical fields. Nevertheless, unlike geometrical and wave optics, currently there is no text (to my knowledge) devoted to this topic.

This book aims to be the first by presenting current approaches for simulating random optical fields with prescribed statistical properties. In particular, this text demonstrates how to generate optical fields, which are sample functions drawn from a random process described by a correlation function. These random fields can then be used in simulations of optical systems, propagation through random or complex media, scattering from surfaces, etc., which are described in other computational optics texts, like *Computational Fourier Optics* (SPIE Press, 2011), *Optics Using MATLAB*[®] (SPIE Press, 2017), *Numerical Simulation of Optical Wave Propagation* (SPIE Press, 2010), *Computational Methods for Electromagnetic and Optical Systems* (CRC Press, 2011), and *Computational Photonics* (Wiley, 2010).

The secondary purpose of this book is as a teaching tool, augmenting the theoretical concepts presented in Wolf’s and Goodman’s classic texts. Traditionally, students of optics begin with geometrical and wave optics, which are taught assuming deterministic optical fields. The transition to the concept of a random optical field can be difficult to grasp, especially when the mathematics requires understanding and applying random process theory. On the other hand, by generating realizations of the random optical field, the statistical optics problem simplifies to a deterministic geometrical or wave optics problem with which students are more familiar. In the context of statistical optics, this simulation is a single random experiment, and statistical moments are computed from the outcomes of many such independent experiments. It has been my experience that this Monte Carlo approach to statistical optics provides a significant amount of insight into the underlying physical phenomena, which greatly exceeds that from theory alone.

This book is intended for senior undergraduate- and graduate-level students studying optical physics and engineering as well as researchers or engineers working in optics. The topics covered in this text require a working knowledge of differential and integral calculus, probability and statistics, random processes, linear systems, and MATLAB[®] programming. It is impossible to include all the background information on a topic as broad as statistical optics and keep the text at a manageable length. Therefore, this book includes extensive reference lists where many of these details can be found.

This textbook is organized into six chapters and three appendices. Chapter 1 briefly reviews scalar diffraction theory—including the plane wave spectrum, Rayleigh–Sommerfeld, Fresnel, and Fraunhofer diffraction—before discussing the foundational principles of scalar statistical optics. We begin with the first-order or single-point statistics of polarized thermal and pseudo-thermal light, presenting the probability density functions (PDFs) and statistical moments of the instantaneous field and irradiance. We then proceed to second-order (two-point) statistics of the optical field and review key concepts such as the mutual coherence function, cross-spectral density (CSD) function, the coherent-modes representation of the CSD function, the superposition rule, and the van Cittert–Zernike theorem. We close the chapter with a review of second-order irradiance statistics of thermal light sources, including the covariance of irradiance, integrated irradiance, and intensity interferometry also known as the Hanbury Brown and Twiss effect.

In Chapter 2, we present several methods for generating random scalar fields given a CSD function. These simulation techniques include coherent modes, pseudo-modes, and the superposition rule. Step-by-step instructions are provided for implementing each of these techniques, and we generate multiple random sources using these algorithms. All of the MATLAB scripts are explained in detail prior to analyzing the results, and the source code is provided in Appendix C and electronically as part of this book (see supplemental material .

Chapter 3 generalizes the theory presented in Chapter 1 to vector or electromagnetic random fields. In this chapter, we begin by reviewing vector diffraction theory, the polarization ellipse, Jones vectors, Stokes parameters, and the Poincaré sphere. We then proceed to the first-order statistics of partially polarized thermal light and discuss such concepts as the coherency matrix, the degree of polarization, the polarization state of random fields, and the PDFs of the Stokes parameters. This is followed, quite naturally, by a review of the second-order moments of the optical field. The topics presented here are the beam coherence-polarization matrix (BCPM), the CSD matrix (CSDM), the electromagnetic coherent-modes representation, bimodal expansions of the CSDM, and the electromagnetic superposition rule. Lastly, we conclude the chapter with a brief summary of second-order irradiance statistics of partially polarized thermal light sources.

Chapter 4 discusses several methods for generating random electromagnetic fields, including bimodal expansions, vector pseudo-modes, and the electromagnetic superposition rule. Like in Chapter 2, step-by-step instructions are provided for implementing each of these techniques, and we generate example electromagnetic random sources using these algorithms. All of the MATLAB scripts are explained in detail.

In Chapter 5, we apply the concepts and algorithms from the prior chapters to analyze and simulate classical statistical optics experiments and instruments, as well as applications that utilize random light. Included in this chapter are detailed simulations of the double-slit or Young's experiment, a Michelson interferometer, beam and polarization control with stochastic fields, the Hanbury Brown and Twiss experiment, and imaging with partially coherent light.

Chapter 6 describes how to simulate nonstationary or pulsed random fields. Nonstationary partially coherent sources, especially those with space-time or spatiotemporal coupling, have recently gained interest for potential use in optical trapping, optical tweezing, and atomic optics. They are currently at the forefront of beam-control research. What makes simulating nonstationary random fields especially interesting is the ability to observe the time evolution of the source. This can provide significant insight into how random fields behave. We begin this chapter with a summary of the germane theory—including reviews of the BCPM, coherent modes and bimodal expansions of the BCPM, pseudo-modes, and the superposition rule—before generating three example thermal, nonstationary sources. As part of these simulations, we create movies showing the temporal evolution of these random fields, which are included with the MATLAB code that accompanies this book. We discuss the fields' physical behaviors in the text.

Lastly, besides the MATLAB source code in Appendix C, the appendices cover two topics that are generally useful when simulating optical propagation, be it deterministic or random. The first, in Appendix A, explains how to simulate wave propagation through optical systems (described by a ray-tracing **ABCD** matrix) by evaluating the Collins formula, also known as the generalized Huygens–Fresnel integral, using fast Fourier transforms. In the appendix, we derive the sampling constraints for two forms (specifically, the Fourier transform and convolution form) of the Collins formula and present an example where we simulate wave propagation through an astigmatic optical system. In Appendix B, we describe how to simulate fields with high spatial frequency content (spatially broadband fields) via Fresnel spatial filtering. Fields of this type include point sources (deterministic) and spatially incoherent fields (stochastic). We first present the theory underpinning Fresnel spatial filtering and then apply the technique to simulate propagation of a spatially incoherent source.

It has become somewhat of a cliché but is nonetheless true: No one writes a book alone. There are many people that deserve my thanks for making it

possible. First, I would like to acknowledge my Master's research advisor Prof. Michael Havrilla. His insistence on linking the mathematics to physical understanding has motivated all of my work in electromagnetics and optics. Second, I would like to thank my doctoral advisor Dr. Jason Schmidt. He is the most knowledgeable person in numerical wave propagation that I know, and his lessons on the subject heavily influenced this work. These two individuals are the most responsible for giving me the knowledge to write this book, and I am eternally grateful.

Other people that played major roles in this effort are Dr. Santasri Bose-Pillai, Dr. Jack McCrae, and Prof. Steven Fiorino at the Center for Directed Energy of the Air Force Institute of Technology (AFIT) and Dr. Mark Spencer at the Directed Energy Directorate of the Air Force Research Laboratory (AFRL). The latter two have been extremely generous providing financial support for my research. They made many of the simulation topics covered in this book possible. I would also like to thank Prof. David Voelz at New Mexico State University and Prof. Olga Korotkova at the University of Miami for many fruitful research collaborations. I look forward to many more in the future.

Last and certainly not least, I am incredibly grateful for my family—Cristina, Elissa, and Anna. Your patience and understanding while I spent seven days a week for nine months writing this book have been incredible.

Milo Hyde
3 May 2022

Chapter 1

Scalar Partially Coherent Sources: Theoretical Foundations

1.1 Review of Scalar Diffraction Theory

Statistical optics is fundamentally the study of random or stochastic electromagnetic fields. Like all other electromagnetic fields, random fields are solutions to Maxwell's equations. Maxwell's equations are a set of four first-order partial differential equations. The unknowns in the equations are the electric and magnetic fields, which consist of three field or vector components each.

In general, Maxwell's equations couple the components of the electric and magnetic fields together. However, in many scenarios of practical interest, the coupling is weak and can be neglected. This allows each field component to be treated independently, in essence, approximating the vector electromagnetic field as a scalar wave.^{1,2} Here, we review the key concepts of this analysis better known as scalar diffraction theory.

1.1.1 Maxwell's Equations and the Scalar Wave Equation

We begin this summary with Maxwell's equations:³⁻⁷

$$\begin{aligned}\nabla \times \mathbf{E}(\mathbf{r}, t) &= -\mathcal{M}(\mathbf{r}, t) - \mu \frac{\partial}{\partial t} \mathbf{H}(\mathbf{r}, t) \\ \nabla \times \mathbf{H}(\mathbf{r}, t) &= \mathbf{J}(\mathbf{r}, t) + \varepsilon \frac{\partial}{\partial t} \mathbf{E}(\mathbf{r}, t) \\ \nabla \cdot \mathbf{E}(\mathbf{r}, t) &= \frac{\rho_e(\mathbf{r}, t)}{\varepsilon} \\ \nabla \cdot \mathbf{H}(\mathbf{r}, t) &= \frac{\rho_m(\mathbf{r}, t)}{\mu},\end{aligned}\tag{1.1}$$

where \mathbf{E} and \mathbf{H} are the electric and magnetic fields, ρ_e and \mathbf{J} are the electric charge and current densities, ρ_m and \mathcal{M} are the magnetic charge and current

$$\begin{aligned}
U(\mathbf{r}, \omega) &= \frac{\exp(jkz)}{j\lambda z} \iint_{-\infty}^{\infty} U(\boldsymbol{\rho}', \omega) \exp\left(\frac{jk}{2z} |\boldsymbol{\rho} - \boldsymbol{\rho}'|^2\right) d^2\rho' \\
&= \frac{\exp(jkz)}{j\lambda z} \exp\left(\frac{jk}{2z} \rho^2\right) \iint_{-\infty}^{\infty} U(\boldsymbol{\rho}', \omega) \\
&\quad \times \exp\left(\frac{jk}{2z} \rho'^2\right) \exp\left(-\frac{jk}{z} \boldsymbol{\rho} \cdot \boldsymbol{\rho}'\right) d^2\rho',
\end{aligned} \tag{1.27}$$

where the two expressions are the convolution and Fourier transform forms of the Fresnel integral, respectively.¹ For large z , i.e., $z > 2D^2/\lambda$, where D is the diameter or width of $|U|$, the inner quadratic phase factor in Eq. (1.27) can be neglected, simplifying the Fresnel integral to

$$U(\mathbf{r}, \omega) = \frac{\exp(jkz)}{j\lambda z} \exp\left(\frac{jk}{2z} \rho^2\right) \iint_{-\infty}^{\infty} U(\boldsymbol{\rho}', \omega) \exp\left(-\frac{jk}{z} \boldsymbol{\rho} \cdot \boldsymbol{\rho}'\right) d^2\rho'. \tag{1.28}$$

This relation is known as the Fraunhofer, or far-zone propagation integral, and is equivalent to the spatial Fourier transform of U at $z = 0$.¹

1.2 First-Order Field and Irradiance Statistics

In this section, we discuss the first-order statistics of thermal and pseudo-thermal light, both of which are defined below. Here, the term first order means at a single point in space and time. The primary goal of this book is to generate field realizations for use in wave-optics simulations that are physically representative of thermal or pseudo-thermal light. It is therefore important to understand the statistics of these random sources.

1.2.1 Thermal and Pseudo-Thermal Light

The term thermal light describes any light source in which the primary mechanism of light generation is spontaneous emission.^{2,23} Examples of thermal sources include stars, incandescent bulbs, gas discharge lamps, and light emitting diodes (LEDs). The light generated by these sources comes from the electrical or thermal excitation of large numbers of random and independent atoms or molecules, which then relax, emitting photons in the process. Pseudo-thermal light is light that has the same statistical properties as thermal radiation; however, the primary light generation mechanism is not spontaneous emission. The most common example of a pseudo-thermal source is laser light scattered from a moving diffuser or rough surface.

At a single time instance, both thermal and pseudo-thermal sources produce spatial irradiance patterns known as speckle patterns—specifically, fully developed speckle patterns.^{2,32–38} Speckle is formed from the random constructive and destructive interference of light resulting in a random

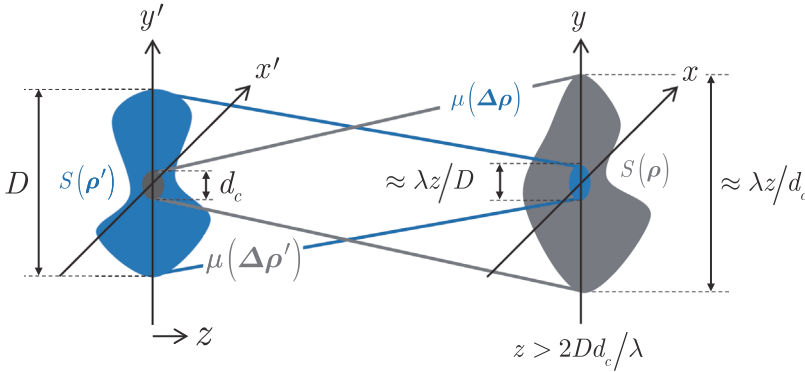


Figure 1.8 Depiction of the generalized van Cittert-Zernike theorem (VCZT).

that we essentially stipulated $d_c \ll D$ by assuming the source-plane field was quasi-homogeneous.

Assuming that Eq. (1.95) holds, the spectral density and SDoC become

$$\begin{aligned}
 S(\mathbf{\rho}, z) &\approx \frac{\tilde{S}(0)}{(\lambda z)^2} \tilde{\mu}\left(\frac{k}{z} \mathbf{\rho}_d\right) \\
 \mu(\mathbf{\rho}_1, \mathbf{\rho}_2, z) &\approx \frac{\exp\left[\frac{jk}{2z}(\rho_1^2 - \rho_2^2)\right]}{\tilde{S}(0)} \tilde{S}\left(\frac{k}{z} \mathbf{\rho}_d\right).
 \end{aligned} \tag{1.96}$$

This result physically states that the observed spectral density is proportional to the Fourier transform of the source-plane μ , and, ignoring the quadratic phase factor, that the observed SDoC is proportional to the Fourier transform of the source-plane S . In other words, the source's shape determines the observation-plane coherence function, and the source's coherence function determines the beam's shape in the observation plane. Figure 1.8 depicts this relationship.

This finding, mathematically expressed in Eq. (1.94), is called the generalized VCZT^{2,34} and is the other fundamental theorem in statistical optics along with the Wiener–Khinchine theorem. A profound implication of the VCZT is that light emitted from an incoherent object gains spatial coherence as it propagates. Applications that use the VCZT are legion: measuring stellar diameters;^{2,23,24,134,135} synthetic aperture imaging,^{2,23,24,134,136} including recently the supermassive black hole M87;¹³⁷ generating partially coherent sources;^{69–71,138–141} and pulse/beam shaping,^{72,142–144} just to name a few.

1.4 Second-Order Irradiance Statistics

When experimenting or in applications dealing with light (all wavelengths shorter than long-wave infrared), we can only sense the light's irradiance or intensity and have no direct access to the optical field. In addition, because

Chapter 2

Simulating Random Scalar Fields

In Chapter 1, we reviewed scalar diffraction theory and the statistics of random light. We observed that the second-order field moments, particularly the mutual coherence function (MCF) and cross-spectral density (CSD) function, obey propagation laws, which are fourfold superposition integrals. Focusing on the CSD function, the propagation law takes the form

$$W(\mathbf{r}_1, \omega_1, \mathbf{r}_2, \omega_2) = \iiint\limits_{-\infty}^{\infty} W(\boldsymbol{\rho}'_1, \omega_1, \boldsymbol{\rho}'_2, \omega_2) \times G(\mathbf{r}_1, \omega_1; \boldsymbol{\rho}'_1) G^*(\mathbf{r}_2, \omega_2; \boldsymbol{\rho}'_2) d^2\rho'_1 d^2\rho'_2, \quad (2.1)$$

where G is the impulse response, or Green's function, modeling the physical system. In most cases, Eq. (2.1) cannot be evaluated analytically and we must turn to a numerical method.

One such numerical approach is to evaluate Eq. (2.1) directly,¹⁻³ which is a daunting task. In the most general case, this requires us to store the source-plane CSD function and G —both six-dimensional functions—and then compute a very large matrix-vector product. Even in cases where the superposition integral can be computed using fast Fourier transforms (FFTs), we still must store the source-plane CSD function and compute a four-dimensional FFT. Needless to say, direct computation of Eq. (2.1) is not easy.

Another numerical approach is to use the coherent-modes expansion or the superposition rule (pseudo-modes) to split the fourfold integral in Eq. (2.1) into the product of two identical double integrals:

realization of an inhomogeneous speckle field provides little insight into the characteristics of the ensemble. Nonetheless, when observed or measured over the ensemble of realizations, the statistics are equivalent to those of a fully developed speckle field.

Nearly all speckle-related research assumes random fields that have homogeneous coherence functions.^{41,55–61} This is because speckle fields of this type occur naturally, i.e., practically any time spatially coherent light scatters from a random interface with roughness on the order of λ . On the other hand, inhomogeneous speckle fields, like Figs. 2.9(e) and (f), are artificial and must be deliberately generated.⁶²

2.2 Superposition Rule: Pseudo-Modes

In the previous section, we discussed three coherent-modes simulation approaches: the random-index, mode-amplitude, and sum-of-modes methods. Here, we present the pseudo-modes (PM) equivalents of the first two; the sum-of-modes equivalent is presented in Section 2.3.

The pseudo-modes for a given CSD function are much easier to find than its coherent-modes expansion. Therefore, the methods presented in the next two sections can be used to simulate nearly any random light source. On the other hand, pseudo-modes are not orthogonal, unique, nor discrete. This generally means that a much larger number of pseudo-modes are required to represent a light source than coherent modes.

We discussed pseudo-modal expansions of CSD functions⁶³ in Section 1.3.5. Recall that the superposition rule forms the basis for the derivation of pseudo-modes:

$$W(\mathbf{r}_1, \mathbf{r}_2) = \int \int \int_{-\infty}^{\infty} p(\mathbf{v}) H(\mathbf{r}_1, \mathbf{v}) H^*(\mathbf{r}_2, \mathbf{v}) d^3 \mathbf{v}, \quad (2.36)$$

where p and H are nonnegative and kernel functions, respectively.⁶⁴ In the pseudo-modes interpretation of Eq. (2.36), H is the pseudo-mode and p is the weight function. The random-index PM analogue views p as the joint PDF of the random vector \mathbf{v} . The source randomly emits pseudo-modes $H(\mathbf{r}, \mathbf{v})$, with \mathbf{v} drawn from $p(\mathbf{v})$.^{15,27,65–69} The mode-amplitude analogue views p as the effective amplitude of a pseudo-mode. The source radiates a particular $H(\mathbf{r}, \mathbf{v})$ only once, weighted by $\sqrt{p(\mathbf{v})}$.^{27,70–72} Incoherently summing over \mathbf{v} yields the CSD function in Eq. (2.36).

Although these two PM approaches are nearly identical to the corresponding coherent-modes methods, pseudo-modes differ from coherent modes in two key aspects that affect implementation: pseudo-modes are not orthogonal nor are they discrete. As stated above, both of these mean that many more pseudo-modes are required to accurately represent a random source.

$$\begin{aligned}
 P \geq \text{ceil}\left(\frac{L}{\Delta}\right) &= \text{ceil}(2Lf_{\max}) \\
 &= \frac{2L}{\pi} \left[2\sigma W\left(\frac{D_p}{2}\right) \sqrt{-\ln \varepsilon} + \frac{D_p}{2} \gamma \right] = 800.
 \end{aligned} \tag{2.57}$$

Listings 2.9 and 2.10 present the MATLAB code for generating a Lajunen and Saastamoinen self-focusing NUC source using the PM random-index and mode-amplitude methods, respectively. These scripts are essentially the same as Listings 2.7 and 2.8, except for the source particulars (source parameters, pseudo-mode H , and weight function p) as well as the number of modes N and grid points P . Therefore, we do not provide detailed breakdowns of the code as we have in past simulation examples.

Results

The results of the self-focusing NUC source simulations are shown in Figs. 2.18–2.20. Starting with Fig. 2.18, we can clearly see the Gaussian shape and off-axis focus in the field realizations. Figure 2.19 shows the source-plane spectral density results. Like the BGCSM S results, the PM random-index and mode-amplitude S are numerically identical to theory. This is because the beam shape s is the only part of H that impacts the source-plane spectral density. Lastly, Fig. 2.20 displays the CSD function results: (g) shows the $x_2 = -x_1 + 2\gamma_x$ slices through $\text{Re}(W)$. These slices run along the anti-diagonal “spurs” in (a), (c), and (e). Artifacts are visible in the random-index method results shown in Figs. 2.20(c) and (d). As was the case for the BGCSM simulations, the speckle contrast provides a good estimate for the magnitude of these errors.

2.3 Superposition Rule: Thermal and Pseudo-Thermal Light

In the previous section, we explored two pseudo-modes simulation techniques that were direct analogues of the random-index and mode-amplitude coherent-modes methods. Both of these methods produced optical field realizations consistent with a desired CSD function. However, since the fields were not thermal, other moments, such as the mean field and covariance of irradiance, were generally nonphysical. If our primary interest is the second-order field moments, this drawback means little and it makes sense to use the coherent-modes (if known) or pseudo-modes methods described in prior sections. If, on the other hand, it is important that the optical field realization be thermal, the random-index and mode-amplitude methods simply cannot be used.

$\sqrt{p(\mathbf{v})}$ and $H(L/2, \mathbf{v})$ with respect to \mathbf{v} , find $f_{v,\max}$, and $N \geq \text{ceil}(D_p/\Delta_v) = \text{ceil}(2D_p f_{v,\max})$, where D_p is the width of \sqrt{p} . Note that \sqrt{p} decreases $f_{v,\max}$ by about the same amount as it increases D_p ; therefore, N is approximately equal to the PM random-index and mode-amplitude methods. Lastly, the procedure for finding the number of grid points P is also the same: Fourier transform $H(\mathbf{r}, D_p/2)$ with respect to \mathbf{r} , find f_{\max} , and $P \geq \text{ceil}(L/\Delta) = \text{ceil}(2L f_{\max})$. The number of grid points P for this method is generally greater than the PM random-index and mode-amplitude methods because of the larger D_p .

We have yet to assign a name to this technique. While the PM sum-of-modes moniker seems quite natural and obvious, the field is rarely computed as a pure sum of modes, unlike its coherent-modes analogue. Indeed, the technique is almost always implemented as a matrix-vector product computed using an FFT, and variants of the method (known by several names) have been used for the past several decades to generate seismic data,^{81,86,87} rough surfaces,^{88–92} random optical fields,^{34,93–97} speckle,^{49,50} and turbulent phase screens.^{33,98–102} Although closely related methods predate the actual superposition rule, for our purposes, the name superposition-rule method is apropos and captures its essence.

The procedure for the superposition-rule method is as follows:

Algorithm 2.6. Superposition-rule method

1. Identify W with known pseudo-mode (impulse response) H and weight function p .
2. Determine the number of pseudo-modes (grid points in the \mathbf{v} domain) N required to approximate the source by applying the sampling criterion to \sqrt{p} and H with respect to \mathbf{v} .
3. Determine the number of grid points P required to discretize H by applying the sampling criterion with respect to \mathbf{r} .
4. Generate a field realization U using Eq. (2.66).
5. Perform the desired operation on U . This operation could be propagating U through an optical system, complex media, etc. Note that the operation's impulse response G must be properly sampled.
6. Compute trial moments.
7. Repeat steps 4–6 at least M times [see Eq. (2.19)].
8. Average the trial moments.

2.3.2 Schell-Model Sources

Like all the other methods we have discussed, we begin with a planar SM source. Recall that for SM sources,

$$H(\boldsymbol{\rho}, \mathbf{v}) = s(\boldsymbol{\rho}) \exp(j\mathbf{v} \cdot \boldsymbol{\rho}), \quad (2.67)$$

Chapter 3

Electromagnetic Partially Coherent Sources: Theoretical Foundations

3.1 Review of Electromagnetic Theory

In Chapter 1, we reviewed important concepts in scalar diffraction theory and statistical optics. While incredibly insightful and an accurate approximation (in many practical scenarios), scalar statistical optics misses important physical phenomena, such as partial polarization and coherence-induced polarization changes. Here, we generalize the scalar concepts discussed in Chapter 1 to account for light being an electromagnetic wave.

Following the outline of Chapter 1, we begin with a brief review of electromagnetic diffraction theory. Using the electromagnetic form of the plane wave spectrum, we derive the Rayleigh–Sommerfeld electromagnetic diffraction integrals for both the electric and magnetic fields. We discuss the paraxial near-field and non-paraxial far-field approximations to these integrals and their affect on polarization. Moving away from diffraction, we conclude the section by examining polarization in a more general context. We review the polarization ellipse, Jones vectors and matrices, Stokes parameters, Mueller matrices, and finally, the Poincaré sphere, as these concepts will be useful in our subsequent analyses of random electromagnetic beams.

3.1.1 Electromagnetic Plane Wave Spectrum

Let us return to the vector wave equation and derive a general expression for the electromagnetic field at any location in the half-space $z \geq 0$:

$$\nabla^2 \mathbf{E}(\mathbf{r}, t) = \frac{\epsilon_r \mu_r}{c^2} \frac{\partial^2}{\partial t^2} \mathbf{E}(\mathbf{r}, t), \quad (3.1)$$

where $c = 1/\sqrt{\epsilon_0 \mu_0}$ is the speed of light in vacuum and ϵ_r and μ_r are the relative permittivity and permeability of the medium; they are related to the index of refraction by $n = \sqrt{\epsilon_r \mu_r}$.¹⁻⁷

propagating in the z direction) are changing rapidly (on the order of the coherence time) and independently of each other. We know from the analysis presented in this section that the polarization state depends on the relationship between the x and y electric field components. Thus, the polarization state of light emitted by this source varies rapidly, where $S_1 \approx S_2 \approx S_3 \approx 0$ when measured over a realistic detector integration time. Light in this state is called unpolarized or randomly polarized.

Both Jones vectors (generalized to the coherency matrix) and Stokes parameters can accommodate stochastic sources by averaging over vector field realizations. We review this analysis in the following sections.

3.2 First-Order Field and Irradiance Statistics

Like in Chapter 1, we begin our discussion of stochastic light with the first-order statistics of thermal and pseudo-thermal electromagnetic fields. By first order, we again mean at a single point in space and time. For this topic, we will generalize Jones vectors and Stokes parameters to include stochastic electromagnetic fields. We will also find the probability density functions (PDFs) for partially polarized light and the elements of the Stokes vector.

3.2.1 Partially Polarized Thermal and Pseudo-Thermal Light

Recall that in Section 1.2.2, we obtained the PDFs of irradiance for polarized and unpolarized thermal and pseudo-thermal light. We were able to easily derive the latter from the former because, for unpolarized thermal light (called natural light), the two basis polarization states (the x and y linear states, for instance) are independent and identically distributed.^{11,33,34,51,52} Thus, the PDF of irradiance for unpolarized light is the sum of two independent exponential random variables. This PDF is easy to compute using a random variable transformation.

For the general case of partially polarized light, however, the two basis polarization states (hereafter, assumed to be the x and y linear states) are not independent. The simplest way to deal with the correlation between the x and y states is through the coherency matrix introduced by Wiener⁵³ and Wolf.⁵⁴ The coherency matrix is defined as the ensemble (or time) average of the outer product of the Jones vector, namely,

$$\begin{aligned}
 \mathbf{J}(\mathbf{r}, t) &= \left\langle \begin{bmatrix} E_x(\mathbf{r}, t) \\ E_y(\mathbf{r}, t) \end{bmatrix} \begin{bmatrix} E_x(\mathbf{r}, t) \\ E_y(\mathbf{r}, t) \end{bmatrix}^\dagger \right\rangle \\
 &= \begin{bmatrix} \langle |E_x(\mathbf{r}, t)|^2 \rangle & \langle E_x(\mathbf{r}, t) E_y^*(\mathbf{r}, t) \rangle \\ \langle E_x^*(\mathbf{r}, t) E_y(\mathbf{r}, t) \rangle & \langle |E_y(\mathbf{r}, t)|^2 \rangle \end{bmatrix} \\
 &= \begin{bmatrix} J_{xx} & J_{xy} \\ J_{xy}^* & J_{yy} \end{bmatrix},
 \end{aligned} \tag{3.58}$$

$$\begin{aligned}
p_{S_i}(S_i) &= [\langle S_0 \rangle^2 (1 - \mathcal{P}^2) + \langle S_i \rangle^2]^{-1/2} \\
&\times \exp \left\{ \frac{-2|S_i|}{\langle S_0 \rangle^2 (1 - \mathcal{P}^2)} \left[\sqrt{\langle S_0 \rangle^2 (1 - \mathcal{P}^2) + \langle S_i \rangle^2} - \text{sgn}(S_i) \langle S_i \rangle \right] \right\},
\end{aligned} \tag{3.96}$$

where $i = 1, 2, 3$.

3.3 Second-Order Field Statistics

Continuing to follow the outline of Chapter 1, we now discuss second-order moments of the electromagnetic field. As a reminder, by “second order” we mean the average behavior of the field at two points in space and time, i.e., \mathbf{r}_1 , \mathbf{r}_2 , t_1 , and t_2 . We begin by presenting the two-point generalization of the coherency matrix, better known as the beam coherence-polarization matrix (BCPM). We then introduce its Fourier transform, i.e., the cross-spectral density matrix (CSDM), and spend the remainder of the section discussing important concepts applicable to the CSDM. Lastly, we discuss important CSDM models, which we simulate in Chapter 4.

3.3.1 Beam Coherence-Polarization Matrix

The first theoretical treatment of the second-order properties of random electromagnetic fields was presented by Emil Wolf in 1954.⁶⁷ Wolf’s general theory uses four 3×3 correlation or coherence matrices formed from $\langle \mathbf{E}(\mathbf{r}_1, t_1) \mathbf{E}^\dagger(\mathbf{r}_2, t_2) \rangle$, $\langle \mathbf{H}(\mathbf{r}_1, t_1) \mathbf{H}^\dagger(\mathbf{r}_2, t_2) \rangle$, $\langle \mathbf{E}(\mathbf{r}_1, t_1) \mathbf{H}^\dagger(\mathbf{r}_2, t_2) \rangle$, and $\langle \mathbf{H}(\mathbf{r}_1, t_1) \mathbf{E}^\dagger(\mathbf{r}_2, t_2) \rangle$. These are called the electric, magnetic, and mixed coherence matrices, respectively, and each satisfies a pair of wave equations in free space.^{11,67,68}

For beam-like or paraxial fields, Wolf’s general treatment simplifies considerably. From Section 3.1.1, we know that for paraxial light the field is approximately transverse electromagnetic (TEM) to the direction of propagation (hereafter assumed to be z). Thus, only the transverse (x and y) components of the field are significant, and Wolf’s 3×3 matrices reduce to 2×2 matrices. In addition, the magnetic field \mathbf{H} is proportional to \mathbf{E} [see Eq. (3.24)]. Consequently, only the electric coherence matrix is necessary.

The first group to present this theory was Gori et al.,^{69,70} who defined the BCPM as a “two-point” generalization of the coherency matrix and a vector generalization of the mutual coherence function (MCF). In their treatment, Gori et al. assumed that the field was wide-sense stationary (WSS). The BCPM was subsequently generalized to nonstationary or pulsed fields by Voipio et al.,^{71,72} which is the form we present below:

$$\begin{aligned}
W_{\alpha\beta}(\boldsymbol{\rho}_1, \boldsymbol{\rho}_2) &= \frac{\alpha_1}{2\sigma_\alpha} \exp\left(-\frac{\rho_1^2}{4\sigma_\alpha^2}\right) \frac{\beta_2}{2\sigma_\beta} \exp\left(-\frac{\rho_2^2}{4\sigma_\beta^2}\right) \\
&\times B_{\alpha\beta} \frac{1}{H_{2m}(0)} \exp\left[-\frac{(\rho_1^2 - \rho_2^2)^2}{\delta_{\alpha\beta}^4}\right] H_{2m}\left(\frac{\rho_1^2 - \rho_2^2}{\delta_{\alpha\beta}^2}\right)
\end{aligned} \tag{3.145}$$

- Electromagnetic cosh-Gauss non-uniformly correlated beam:⁹⁶

$$\begin{aligned}
W_{xx,yy}(\boldsymbol{\rho}_1, \boldsymbol{\rho}_2) &= \exp\left(-\frac{\rho_1^2 + \rho_2^2}{4\sigma^2}\right) \left(\exp\left\{-\frac{[f(\boldsymbol{\rho}_1) - f(\boldsymbol{\rho}_2)]^2}{2\delta^4}\right\} \right. \\
&\quad \left. \pm \exp\left\{-\frac{[f(\boldsymbol{\rho}_1) + f(\boldsymbol{\rho}_2)]^2}{2\delta^4}\right\} \cos(2\phi_0) \right) \\
W_{xy}(\boldsymbol{\rho}_1, \boldsymbol{\rho}_2) &= \exp\left(-\frac{\rho_1^2 + \rho_2^2}{4\sigma^2}\right) \exp\left\{-\frac{[f(\boldsymbol{\rho}_1) + f(\boldsymbol{\rho}_2)]^2}{2\delta^4}\right\} \sin(2\phi_0),
\end{aligned} \tag{3.146}$$

where f is a real-valued function ($f = \rho^2$ in Ref. [96]) and ϕ_0 is the phase difference between the x and y field components.

This concludes our summary of popular CSDM models. In the next chapter, we will generate electromagnetic field realizations using a few of these CSDMs.

3.4 Second-Order Irradiance Statistics

In the last section of Chapter 1, we presented a summary of the Hanbury Brown and Twiss (HBT) effect for fully polarized (scalar) fields. Here, we derive an expression for the normalized covariance of irradiance b_I for partially polarized, Gaussian-distributed fields. We do not, however, generalize the integrated irradiance statistics nor the intensity interferometry equations. The primary reason for this is that most intensity interferometry applications involve either polarized or natural light sources.^{34,151,152} We discussed the former in Chapter 1. For the latter, the light emitted by the source and subsequently measured by the detectors is unpolarized. We can infer how this affects the scalar, normalized covariance of integrated irradiance b_I [see Eq. (1.124)] from b_I without concern that the detectors integrate the irradiance. If the source emits partially polarized light, the b_I lies between these two extremes. In the brief summary to follow, we return to the space-time domain and make use of the beam coherence-polarization matrix (BCPM). We note that this same analysis has been performed in the space-frequency domain using the CSDM. These references are included in the citations below.

Chapter 4

Simulating Random Electromagnetic Fields

As explained at the beginning of Chapter 2, using the cross-spectral density (CSD) function or the cross-spectral density matrix (CSDM) directly in optical simulations is computationally onerous because of the high dimensionality of these functions. Take, for instance, the propagation equation for the CSDM of a wide-sense stationary (WSS) electromagnetic field:

$$\mathbf{W}(\mathbf{r}_1, \mathbf{r}_2, \omega) = \iiint \int_{-\infty}^{\infty} \mathbf{K}(\mathbf{r}_1, \omega; \boldsymbol{\rho}'_1) \mathbf{W}_\rho(\boldsymbol{\rho}'_1, \boldsymbol{\rho}'_2, \omega) \times \mathbf{K}^\dagger(\mathbf{r}_2, \omega; \boldsymbol{\rho}'_2) d^2\rho'_1 d^2\rho'_2, \quad (4.1)$$

where \mathbf{K} is the free-space dyadic Green's function¹⁻⁴ and \mathbf{W}_ρ is the 2×2 “transverse” CSDM defined as

$$\mathbf{W}_\rho(\boldsymbol{\rho}_1, \boldsymbol{\rho}_2, \omega) = \left\langle \begin{bmatrix} E_x(\boldsymbol{\rho}_1, \omega) \\ E_y(\boldsymbol{\rho}_1, \omega) \end{bmatrix} \begin{bmatrix} E_x(\boldsymbol{\rho}_2, \omega) \\ E_y(\boldsymbol{\rho}_2, \omega) \end{bmatrix}^\dagger \right\rangle. \quad (4.2)$$

Evaluating the fourfold superposition integral in Eq. (4.1) yields the exact, full 3×3 CSDM at any location in the half-space $z \geq 0$.⁵

In most cases, Eq. (4.1) does not permit a closed-form answer, and evaluating the integrals numerically requires storing and then computing a series of extremely large matrix-vector products. The matrices representing the components of \mathbf{K} are ten dimensional, with every combination of observation points $(x_1, y_1, z_1$ and $x_2, y_2, z_2)$ column-wise and every combination of source points $(x'_1, y'_1$ and $x'_2, y'_2)$ row-wise. The input and output CSDMs are composed of four, four-dimensional and nine, six-dimensional functions, respectively. Even in the case of paraxial propagation, the kernel is eight dimensional and the input and output CSDMs are four dimensional. Computing the superposition integral using fast Fourier transforms (FFTs) results in tremendous memory and run-time savings; however, we still must

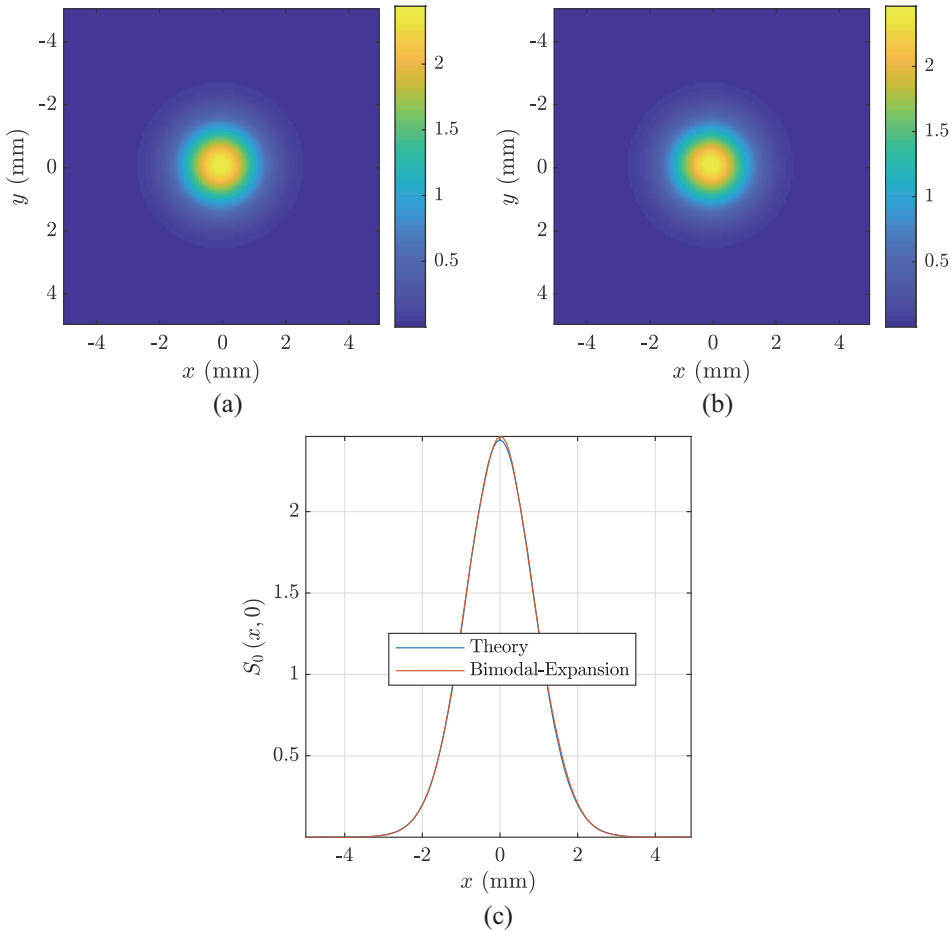


Figure 4.5 EGSM source Stokes parameter S_0 results: (a) theory, (b) bimodal-expansion, and (c) all results $S_0(x, 0)$.

and 4.11(e) and (f), respectively. Like similar artifacts observed in the results in Chapter 2, these will lessen with more trials.

4.2 Superposition Rule: Pseudo-Modes

In the last section, we presented the bimodal-expansion algorithm, which was, in effect, a generalized version of the sum-of-modes method (see Section 2.1.1). The primary limitation of this algorithm, and the other coherent-modes-based methods, is that the coherent-modes representations for W_{xx} and W_{yy} must be known, either numerically³⁹ or in closed form, and few are.

On the other hand and as was the case for scalar fields, the superposition rule can be used to generate field realizations consistent with any genuine CSDM. In this section, we describe how to simulate random sources using

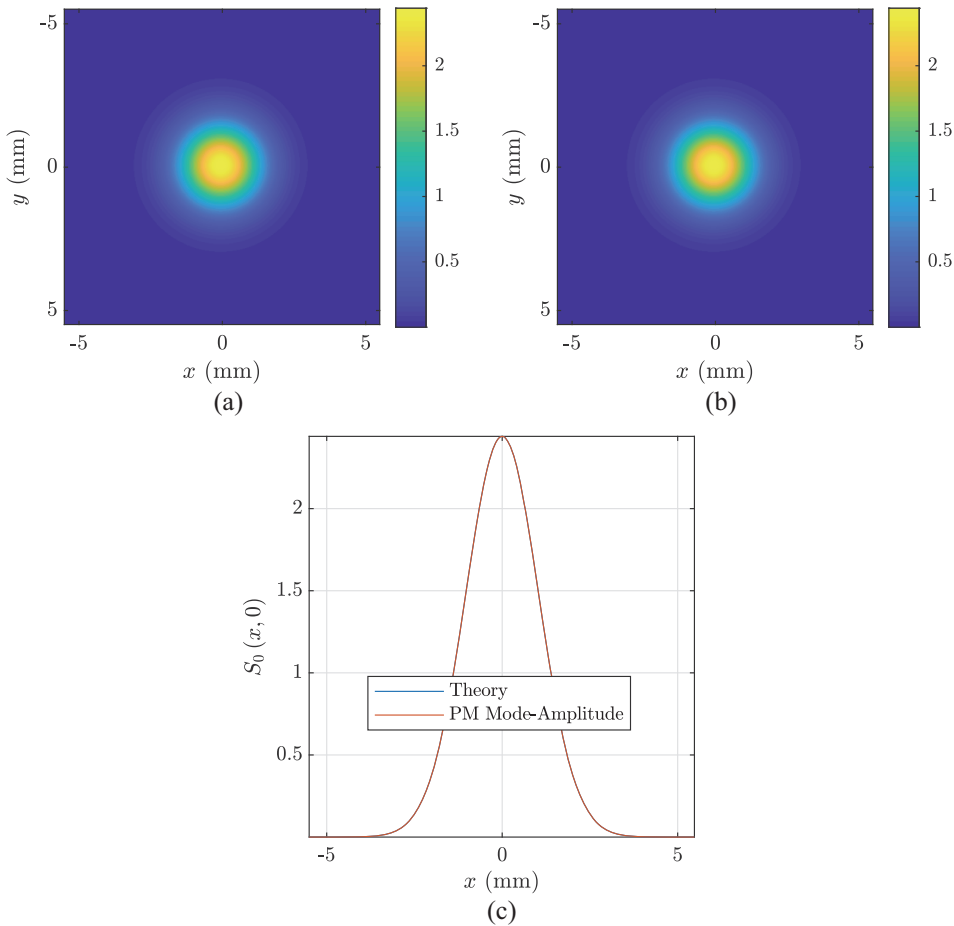


Figure 4.26 Electromagnetic Lajunen and Saastamoinen self-focusing NUC source Stokes parameter S_0 results: (a) theory, (b) PM mode-amplitude, and (c) all results $S_0(x, 0)$.

4.3 Superposition Rule: Thermal and Pseudo-thermal Light

In the last two sections, we developed simulation techniques to generate random electromagnetic fields using coherent-modes and pseudo-modes expansions. Both produced fields with accurate second-order moments. Nevertheless, we must know, at a minimum, the scalar coherent-modes representations for W_{xx} and W_{yy} to use the former, and although the latter can be used to generate fields consistent with any genuine cross-spectral density matrix (CSDM), the fields themselves are not thermal.

In this section, we generalize the superposition-rule method from Section 2.3 to generate thermal electromagnetic field realizations consistent with any genuine CSDM. Like the scalar algorithm, the electromagnetic superposition-rule method generates field realizations via matrix-vector products, which can often be computed using fast Fourier transforms (FFTs). After developing the

Chapter 5

Application Examples

So far this book has followed the basic outline where we first reviewed key theoretical concepts in statistical optics, and then presented methods for generating optical field realizations with the proper (or desired) statistics. Here, we apply those concepts from previous chapters to analyze and then simulate classical statistical optics experiments and instruments, as well as applications that utilize random light. We begin this chapter with the double-slit or Young's experiment followed by the Michelson interferometer. We then present beam shaping and polarization control with stochastic light, before simulating Hanbury Brown and Twiss' famous intensity interferometry experiment from the 1950s. We close the chapter with imaging and partially coherent light.

5.1 Young's Experiment

One of the most influential experiments in the history of both classical and modern physics is the double-slit experiment, also known as Young's experiment.¹⁻³ In this section, we simulate Young's experiment assuming a scalar partially coherent, both temporally and spatially, wide-sense stationary (WSS) light source. The geometry of the experiment is shown in Fig. 5.1. The field emitted from an LED propagates a distance f_1 and is incident on a spherical lens of focal length f_1 . Immediately thereafter, the light passes through two rectangular holes in an opaque screen (dimensions annotated in the figure) and then through another spherical lens of focal length f_2 . We observe the irradiance a distance f_2 from the screen or $f_1 + f_2$ from the source plane.

5.1.1 Theory

The field, immediately before the first spherical lens, is predicted by the Fresnel diffraction integral, namely,

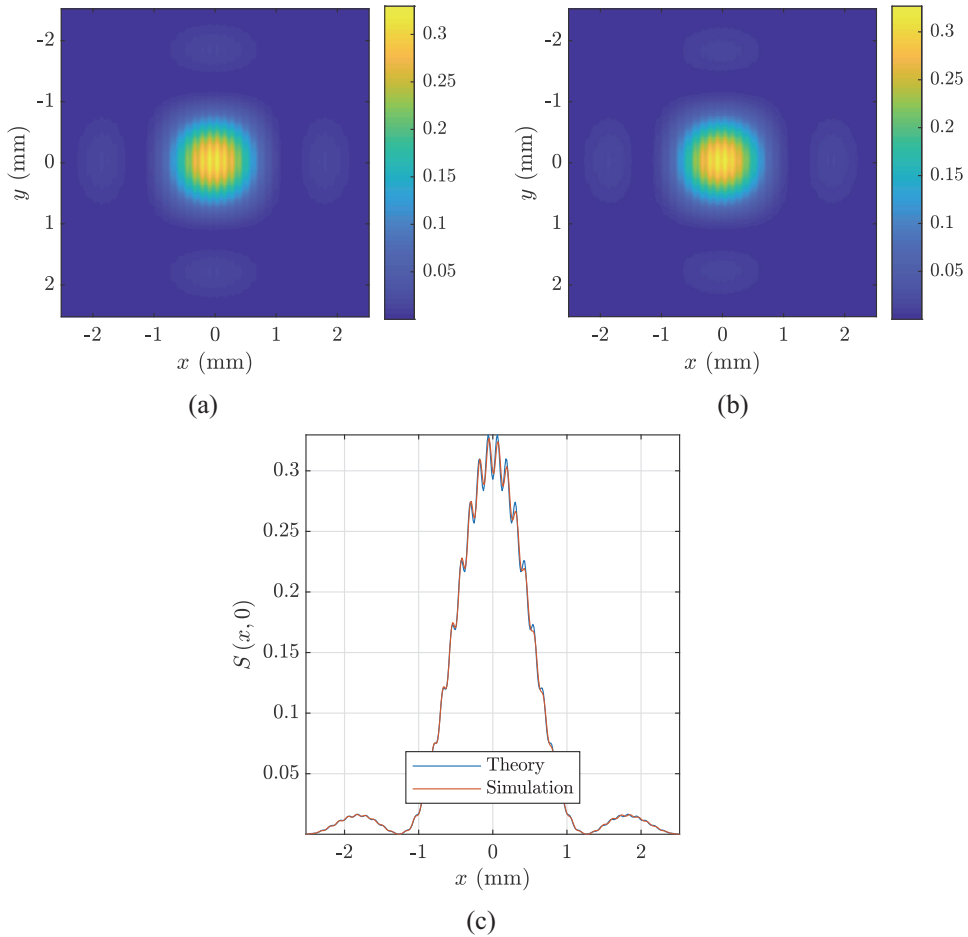


Figure 5.5 Observation-plane spectral density for $L = 4\lambda_c f_1 / (3D)$: (a) theory [see Eq. (5.11)], (b) simulation, and (c) all results $S(x, 0)$.

coherence). For $x > 0.5$ mm, the fringe amplitudes for the theoretical and simulated $\langle I \rangle$ are clearly less than the theoretical S and continue to decrease as x increases.

5.2 Michelson Interferometer

Another incredibly influential experiment—certainly the most famous null result—in the history of physics was the Michelson–Morley experiment.²³ In 1887, A. Michelson and E. Morley used what is now known as a Michelson interferometer to measure the speed of light along two perpendicular paths in an attempt to detect Earth’s movement through the aether. The null result of this experiment is credited with providing the first evidence against the existence of the aether and for the universality of the speed of light and special relativity.

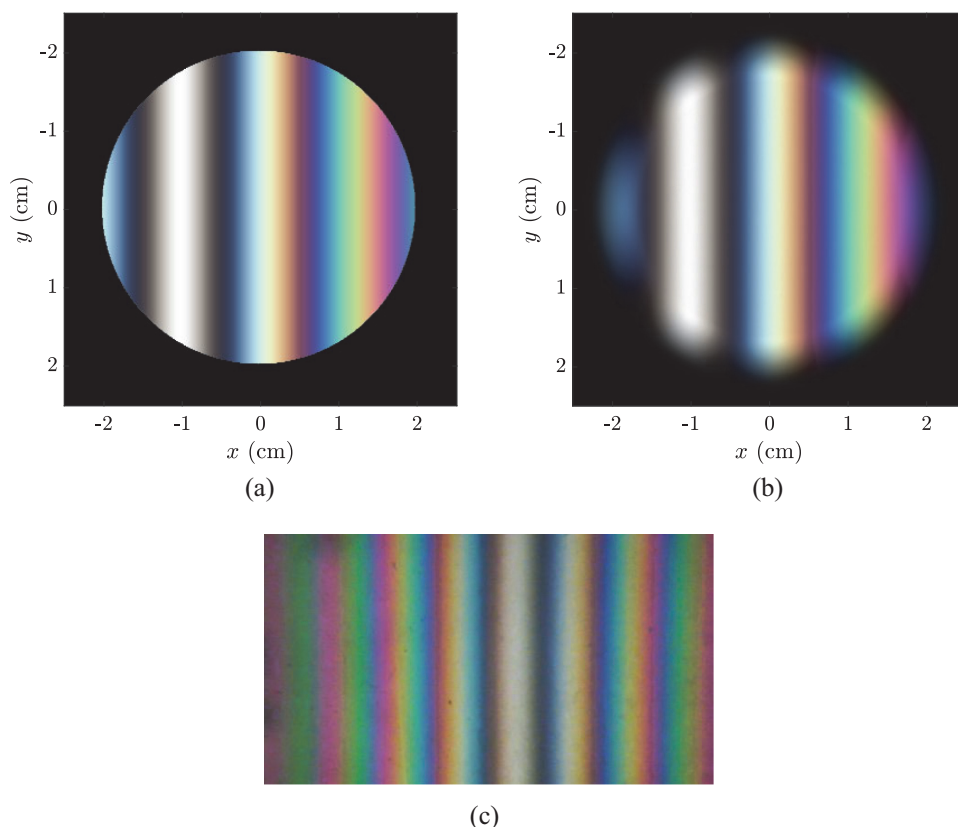


Figure 5.10 Michelson interferometer observation-plane irradiance $\langle I \rangle$ color image (white-light fringes): (a) theory, (b) simulation, and (c) measurement obtained with permission from Prof. Olivier Granier.³³

5.3 The van Cittert–Zernike Theorem

In this section, we demonstrate beam shaping using spatial coherence. Both techniques described below apply the generalized van Cittert–Zernike theorem (VCZT)^{5,6,10,11} for beam control. Figure 5.11 shows the simple geometry employed by both beam-shaping methods. A spatially random field in the $z = 0$ plane (i.e., the source plane) is immediately incident upon a spherical lens of focal length f . We observe the spectral density in the focal plane of the lens $z = f$. Our goal in the first method is to design the random source, such that it emits a beam with the desired ensemble-averaged shape (spectral density) in the $z = f$ plane (the Celtic cross image shown in Fig. 5.11).^{36–38} Indeed, the image shown in Fig. 1.1(b) was generated using this technique.

For the second method, we design an electromagnetic random source that emits a field with customizable polarization ellipse parameters (S_0 , \mathcal{P} , ψ , and χ) in the $z = f$ plane (the sequence of four images in Fig. 5.11).^{39,40} Note that the desired beam shapes/images in Fig. 5.11 do not have much practical use.

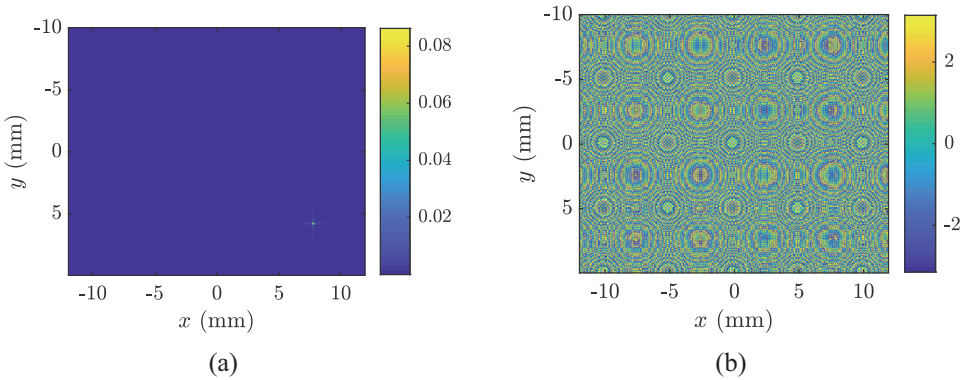


Figure 5.16 Polarization control E_{ax} field realization: (a) $|E_{ax}|$ and (b) $\arg(E_{ax})$.

Results

Figure 5.16 shows a field realization for the E_a pseudo-mode given in Eq. (4.43). The other pseudo-modes, E_b and E_c , look identical. Note that the pseudo-modes' magnitudes are spatially shifted sinc functions. Thus, W_{xx} , W_{yy} , and W_{xy} from Eq. (5.63), and subsequently the Stokes parameters in Eq. (5.64) and polarization ellipse parameters in Eq. (5.66), are formed from the incoherent sums of many shifted sincs. The phase in Fig. 5.16(b) is badly aliased and nonphysical; however, it is irrelevant in our simulation since the phases of H_x and H_y [see Eq. (5.69)] negate each other when computing the Stokes parameters. The phase differences between the x and y electric field components, required for S_2 , S_3 , ψ , and χ , are accurate, as that information is carried in the pseudo-modes' ν -dependent complex amplitudes.

Figures 5.17–5.20 show the S_0 , \mathcal{P} , ψ , and χ results, respectively. The figures are organized in the following manner: (a) shows the desired polarization ellipse parameter, (b) and (c) show the theoretical and simulated results, and (d) displays the pixel-value histograms of (a–c). The results are generally as expected: sharp features in (a) are lost in (b) and (c) due to the finite size of the SLM. This observation holds for \mathcal{P} , ψ , and χ even though they are nonlinearly related to the Stokes parameters and p_{xx} , p_{yy} , and p_{xy} . The S_0 histograms in Fig. 5.17(d) are consistent with the scalar beam-shaping result in Fig. 5.13(d). The histograms for the other polarization ellipse parameters are harder to interpret because of the aforementioned nonlinear relationships between \mathcal{P} , ψ , and χ and ultimately p_{xx} , p_{yy} , and p_{xy} .

5.4 The Hanbury Brown and Twiss Effect

In Section 1.4, we discussed the second-order irradiance moments of thermal scalar fields. We also presented the classical theory underpinning the Hanbury Brown and Twiss (HBT) effect. In this section, we simulate R. Hanbury Brown and R. Q. Twiss' experiment from their 1958 paper in the *Proceedings*

good match to theory and therefore show that our procedure for simulating HBT's experiment is sound.

5.5 Imaging with Partially Coherent Light

For our final application example, we simulate imaging with partially coherent light. Consider the geometry in Fig. 5.23. A rough (on the order of a wavelength) object or target is illuminated with narrowband, partially coherent light. The light scattered from the object propagates a distance z_o to the entrance pupil of the imaging system. Light emerges from the system forming an image of the target at a distance z_i from the exit pupil.

In an imaging system, the entrance and exit pupils are the object-space and image-space images of the most wavefront-limiting element contained in the system.^{4,75} As described by Goodman and Gaskill,^{4,45} with knowledge of the pupils, the contents of the imaging system are generally immaterial. We can model the imager as a “black box” terminated at the entrance and exit pupil planes.

5.5.1 Theory

Following Goodman, Gaskill, and many others,^{4,5,11,43–45,76} the field in the image plane is approximately (neglecting constant and quadratic phase terms)

$$U_i(\mathbf{\rho}_i) \approx \iint_{-\infty}^{\infty} \frac{1}{|M|} U_o\left(\frac{\mathbf{\rho}_o}{M}\right) h(\mathbf{\rho}_i - \mathbf{\rho}_o) d^2\rho_o, \quad (5.86)$$

where M is the transverse magnification and U_o is the light scattered from the object. The kernel h is the amplitude spread function and is given by

$$h(\mathbf{\rho}_i - \mathbf{\rho}_o) = \frac{1}{(\lambda z_i)^2} \iint_{-\infty}^{\infty} \mathcal{P}(\mathbf{\rho}_p) \exp\left[-j\frac{k}{z_i}(\mathbf{\rho}_i - \mathbf{\rho}_o) \cdot \mathbf{\rho}_p\right] d^2\rho_p, \quad (5.87)$$

where \mathcal{P} is the generalized pupil function, i.e.,

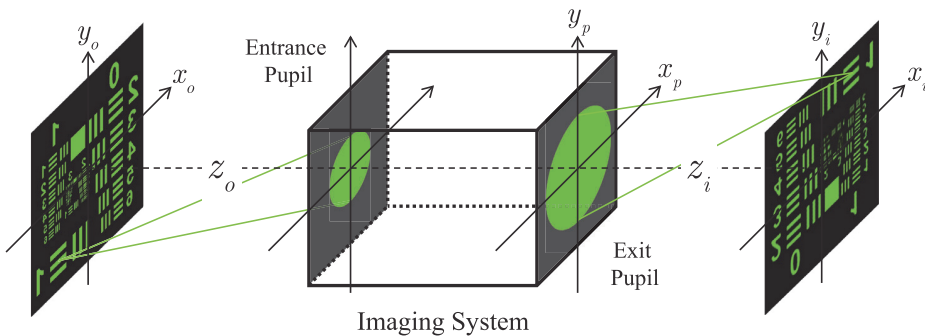


Figure 5.23 Geometry of an imaging system.

Chapter 6

Pulsed Partially Coherent Fields

For a majority of this book and in all the simulations, we have assumed that the random field is wide-sense stationary (WSS). Implied from its definition (see Section 1.3.1), a WSS field must be “on” for all time and is delta-correlated in frequency ω . Indeed, not having to consider correlation between temporal frequency components is why, to this point, we have generated all random fields in the ω domain using the cross-spectral density (CSD) function or cross-spectral density matrix (CSDM). Simulating only sources that have been radiating for all time clearly excludes important physical phenomena, such as temporally shaped or pulsed fields. In addition, simulating nonstationary sources allows one to model real-time optical systems and fast detectors.

In this chapter, we describe how to simulate nonstationary, or pulsed, random fields. These fields can be simulated in the frequency or time domains; however, here we focus on the latter. Simulating the time evolution of thermal (or pseudo-thermal) sources provides insights into how random fields actually behave and can therefore be a valuable pedagogical tool. These insights are generally not available from ω -domain simulations.

We begin with a brief summary of the pertinent theory, which primarily concerns the beam coherence-polarization matrix (BCPM) Γ from Chapter 3. Continuing to follow the general outline of Chapter 3, we then present coherent-modes and bimodal expansions of Γ before concluding with the superposition rule. Like for WSS fields in Chapters 2 and 4, all of these theoretical concepts can be adapted to simulate nonstationary sources. Nonetheless, only simulation techniques derived from the superposition rule are widely applicable, and of those, only the “superposition-rule method” produces thermal (physically representative) field realizations. Consequently, we focus on simulating pulsed random fields using that method. We conclude this chapter by generating three nonstationary sources: a pulsed Schell-model (SM) beam, a non-uniformly correlated (NUC) beam, and a space-time coupled beam.

6.2 Superposition Rule: Thermal and Pseudo-Thermal Light

In this section, we generate three nonstationary random sources using the superposition-rule method. All three have H_α of the form

$$H_\alpha(\mathbf{\rho}, t; \mathbf{v}, v_t) = s_\alpha(\mathbf{\rho}, t) \exp(-j\omega_c t) \exp[j\mathbf{v} \cdot \mathbf{f}(\mathbf{\rho}, t)] \exp[-jv_t g(\mathbf{\rho}, t)]: \quad (6.25)$$

s_α is the field's deterministic space-time pulse shape; $\exp(-j\omega_c t)$ is the sinusoidal oscillation of the field at mean, carrier, or optical frequency ω_c ; and \mathbf{f} and g are arbitrary functions. If \mathbf{f} and g are functions of both position and time (as shown), then the field possesses random space-time (spatiotemporal) coupling.^{37,38} Note that this is physically different from the deterministic spatiotemporal coupling induced (potentially) via s_α .^{39–41}

Regarding $\exp(-j\omega_c t)$, typically, $\omega_c \gg \Delta\omega$ (where $\Delta\omega$ is the field's bandwidth), and therefore, simulating the actual sinusoidal oscillation of the field is prohibitively expensive. In addition, the bandwidths of the fastest detectors are many orders of magnitude smaller than $\omega_c \sim 10^{14}$ Hz. Consequently, we cannot measure the field's oscillation, and simulating it makes even less sense. Because of these factors, we neglect the $\exp(-j\omega_c t)$ term and simulate only the time-changing complex envelope of the field.

Ignoring the “carrier” term has physical consequences that we must account for, if the simulation is to yield accurate results. In particular, we need to modify the diffraction integrals in Chapter 1 to propagate the field's complex envelope. Let us return to the time-domain form of the Rayleigh–Sommerfeld diffraction integral in Eq. (1.21), reproduced here for convenience:

$$U(\mathbf{r}, t) = \frac{1}{2\pi v_p} \iint_{-\infty}^{\infty} \frac{z}{|\mathbf{r} - \mathbf{\rho}'|^2} \frac{\partial}{\partial t} U\left(\mathbf{\rho}', t - \frac{|\mathbf{r} - \mathbf{\rho}'|}{v_p}\right) d^2\mathbf{\rho}' \quad r \gg \lambda, \quad (6.26)$$

where $v_p = 1/\sqrt{\epsilon\mu}$ is the phase velocity in the propagation medium, which we set equal to c hereafter. For paraxial propagation,

$$|\mathbf{r} - \mathbf{\rho}'| \approx \begin{cases} z + \frac{|\mathbf{\rho} - \mathbf{\rho}'|^2}{2z} & \text{“phase” terms} \\ z & \text{“amplitude” terms} \end{cases} \quad (6.27)$$

in Eq. (6.26), respectively. After some simple algebra, Eq. (6.26) becomes

$$U(\mathbf{\rho}, z, t) \approx \frac{1}{2\pi cz} \iint_{-\infty}^{\infty} \frac{\partial}{\partial t} U\left(\mathbf{\rho}', \bar{t} - \frac{\rho'^2}{2zc} + \frac{\mathbf{\rho} \cdot \mathbf{\rho}'}{cz}\right) d^2\mathbf{\rho}', \quad (6.28)$$

where $\bar{t} = t - z/c - \rho^2/(2cz)$ is the time it takes light to propagate from the source to the observation point. If U is narrowband ($\Delta\omega/\omega_c \ll 1$, a condition called quasi-monochromatic), we can write U in terms of its complex envelope U_e , such that^{5,13}

theoretical and simulated $\langle I(0, 0, t) \rangle$. Figures 6.13 and 6.14 are organized in the same manner: (a) and (b) display the real and imaginary parts of the theoretical MCF [see Eq. (6.46)], (c) and (d) show the same for the simulated MCF, and (e) plots the slices through $\text{Re}(\Gamma)$ that run along the anti-diagonal “spurs” in (a) and (c). Overall, there is good agreement between the theoretical and simulated results in these figures, implying that we have successfully generated the desired NUC pulsed beam. The minor artifacts visible in some of the simulated images will fade with more trials.

6.2.3 Spatiotemporal Coupling: Twisted Space-Time Beams

For our last example, we generate a random, scalar nonstationary source with spatiotemporal coupling. Recently, there has been great interest in generating fields with spatiotemporal coupling for possible use in beam control applications, such as optical trapping, optical tweezing, and atomic optics. In the last decade, space-time-coupled beams that possess transverse (to the direction of propagation) angular momentum^{54–62} and anomalous propagation and refractive behaviors^{41,63–67} have been demonstrated. Here, we generate a twisted space-time beam, which is a nonstationary partially coherent field with a stochastic twist^{68,69} coupling its spatial and temporal dimensions.^{70,71} Like the others cited above, a twisted space-time beam carries transverse angular momentum and, as we demonstrate below, rotates or tumbles as it propagates.

To generate this beam, we again follow the steps of Algorithm 2.6. Step 1 is to identify the MCF, p , and H . The MCF for a twisted space-time beam is

$$\begin{aligned} \Gamma(\mathbf{r}_1, t_1, \mathbf{r}_2, t_2) = & A^2 \exp\left(-\frac{y_1^2 + y_2^2}{4\sigma_y^2}\right) \exp\left(-\frac{x_1^2 + x_2^2}{4\sigma_x^2}\right) \exp\left[-\frac{(x_1 - x_2)^2}{2\delta_s^2}\right] \\ & \times \exp\left[-\frac{(t_1 - T_c)^2 + (t_2 - T_c)^2}{4T^2}\right] \exp\left[-\frac{(t_1 - t_2)^2}{2\delta_t^2}\right] \exp[-j\omega_c(t_1 - t_2)] \\ & \times \exp\{-j\mu[x_1(t_2 - T_c) - x_2(t_1 - T_c)]\}, \end{aligned} \quad (6.50)$$

which has a very similar form to a GSM pulsed beam [see Eq. (6.34)]. Indeed, all of the above parameters have the same physical significance as a GSM pulsed beam, with the major exception of μ , which is known as the twist parameter. The twist parameter must satisfy $|\mu|\delta_t\delta_s \leq 1$; consequently, $\mu \rightarrow 0$ in the limit of fully coherent light, i.e., $\delta_t, \delta_s \rightarrow \infty$.^{15,16,69} Referring back to the general form of H given in Eq. (6.25), a twisted space-time beam has a weight function p , beam shape s , f , and g with the following forms.^{72,73}

Appendix A

Numerical Diffraction Using the Collins Formula

In Chapters 2 and 4, we described how to generate field realizations U given any genuine cross-spectral density (CSD) function or cross-spectral density matrix (CSDM). We spent a significant amount of time discussing how to properly sample U so that it was represented accurately on a discrete grid.

After generating U , a common next step in wave-optics simulations is to propagate or otherwise pass U through a linear optical system modeled by a Green's function or impulse response G , such that

$$U(\mathbf{r}, \omega) = \iint_{-\infty}^{\infty} U(\boldsymbol{\rho}', \omega) G(\mathbf{r}, \omega; \boldsymbol{\rho}') d^2 \boldsymbol{\rho}'. \quad (\text{A.1})$$

What is clear in Eq. (A.1) is that a properly sampled input U does not guarantee an accurate output U . We must also consider G , and in general, it must be properly sampled in both the input and output planes. We encountered similar sampling requirements when we generated fields using the pseudo-modes methods in Sections 2.2 and 4.2.

One of the most common G is free-space propagation. Paraxially, this Green's function is known as the Fresnel impulse response and is shown in Eq. (1.27). Simple analysis begets two forms for the Fresnel diffraction integral: one in the form of a superposition (convolution, since the Fresnel impulse response is space invariant) integral like Eq. (A.1) and the other in the form of a spatial Fourier transform. Although mathematically equivalent, the sampling requirements for the convolution and Fourier transform versions of the Fresnel diffraction integral are different, and both have been extensively studied.¹⁻⁷

For diffraction in general paraxial systems, G is given by the Collins formula.^{1,8} Like the Fresnel diffraction integral, the Collins formula (for optical systems with certain symmetries) can be expressed as either a convolution integral or a spatial Fourier transform.^{9,10} The purpose of this appendix is to derive the sampling criteria for both forms of the Collins formula. We start with a general overview of the Collins diffraction integral and specialize it to an x - y

Appendix B

Simulating Spatially Incoherent Sources

Many thermal light sources, e.g., the sun, incandescent bulbs, and LEDs, have extremely small spatial correlation or coherence widths (on the order of λ).^{1–4} Such sources are well modeled as being spatially incoherent; i.e., we can approximate their complex degree of coherences (CDoCs) or spectral degree of coherences (SDoCs) using a Dirac delta function. Because of their ubiquity in nature, incoherent light sources are critically important in the study and understanding of statistical optics. Indeed, they form the basis of the van Cittert–Zernike theorem (VCZT)^{2–8} and, consequently, all applications derived from it (see Section 1.3.7).

When it comes to simulating spatially incoherent sources, we run into a problem: A spatially incoherent source has infinite spatial frequency content. Stated another way, it is not possible to represent a Dirac delta function on a discrete grid. Even if we were to model a spatially incoherent source as a matrix of independent circular complex Gaussian (CCG) random numbers, the correlation radius of our simulated field would equal the grid spacing. Quite simply, this means that in a wave-optics simulation, a spatially band-limited version of an incoherent source must ultimately suffice.

In this appendix, we present a method to simulate spatially incoherent or “near” incoherent sources. Much like simulating point sources in coherent wave-optics simulations,^{9–13} the method presented here reduces the source’s spatial bandwidth via filtering, such that the field emitted by the filtered (or spatially bandlimited) source, after propagating a distance z , has the same cross-spectral density (CSD) function over a specified region of interest as the field emitted by the incoherent source. In the analysis below, we assume frequency ω domain fields and omit the ω dependence of quantities, such as the CSD function, for brevity. Furthermore, we stipulate that all random fields are wide-sense stationary (WSS). We begin by assuming that our source is scalar and quasi-homogeneous; we specialize the result to a spatially incoherent source in the end.

Appendix C

MATLAB[®] Code

Listings

2.1 GSM random-index method simulation example	426
2.2 GSM mode-amplitude method simulation example	427
2.3 GSM sum-of-modes method simulation example	429
2.4 I_m -Bessel random-index method simulation example	430
2.5 I_m -Bessel mode-amplitude method simulation example	432
2.6 I_m -Bessel sum-of-modes method simulation example	433
2.7 BGCSM source PM random-index method simulation example	434
2.8 BGCSM source PM mode-amplitude method simulation example	436
2.9 Self-focusing NUC source PM random-index method simulation example	437
2.10 Self-focusing NUC source PM mode-amplitude method simulation example	438
2.11 MGSM source superposition-rule method simulation example	439
2.12 Self-focusing NUC source superposition-rule method simulation example—direct evaluation of matrix-vector product	440
2.13 Self-focusing NUC source superposition-rule method simulation example—FFT approach	441
4.1 EGSM bimodal-expansion simulation example	443
4.2 EMGSM PM mode-amplitude simulation example using the pseudo-modes in Eq. (4.43)	446
4.3 Electromagnetic self-focusing NUC source PM mode-amplitude simulation example using the pseudo-modes in Eq. (4.36)	448
4.4 EHGCSM source superposition-rule method simulation example	450
4.5 EGPSM source superposition-rule method simulation example	452
5.1 Young's experiment simulation example	454
5.2 Michelson interferometer simulation example	456
5.3 Scalar beam shaping example	459
5.4 Polarization control example	461
5.5 Simulation of Hanbury Brown and Twiss' experiment from Ref. [1]	463



Milo W. Hyde IV received his B.S. degree in computer engineering from the Georgia Institute of Technology, Atlanta, Georgia, in 2001 and his M.S. and Ph.D. degrees in electrical engineering from the Air Force Institute of Technology, Wright-Patterson Air Force Base (AFB), Dayton, Ohio, in 2006 and 2010, respectively.

From 2001 to 2004, he was a maintenance officer with the F-117A Nighthawk, Holloman AFB, Alamogordo, New Mexico; from 2006 to 2007, he was a government researcher with the Air Force Research Laboratory, Wright-Patterson AFB; from 2010 to 2017, he was a Professor in the Department of Electrical and Computer Engineering at the Air Force Institute of Technology; and from 2017 to 2020, he was the United States Air Force Deputy for Operations for the Defense Science Board at the Pentagon, Washington, DC. Currently, he is a Professor in the Department of Engineering Physics at the Air Force Institute of Technology. He has more than 150 journal and conference publications in electromagnetic material characterization, guided-wave theory, and statistical optics.

Dr. Hyde is a member of the Directed Energy Professional Society (DEPS) and a senior member of IEEE, SPIE, and OSA.